

**VICTORIA UNIVERSITY**  
MELBOURNE AUSTRALIA

*Fabrication of novel Janus membrane by nonsolvent thermally induced phase separation (NTIPS) for enhanced performance in membrane distillation*

This is the Accepted version of the following publication

Liu, Y, Xiao, Tonghu, Bao, C, Fu, Y and Yang, Xing (2018) Fabrication of novel Janus membrane by nonsolvent thermally induced phase separation (NTIPS) for enhanced performance in membrane distillation. *Journal of Membrane Science*, 563. 298 - 308. ISSN 0376-7388

The publisher's official version can be found at  
<https://www.sciencedirect.com/science/article/pii/S0376738818308913>  
Note that access to this version may require subscription.

Downloaded from VU Research Repository <https://vuir.vu.edu.au/37726/>



19 **Abstract**

20

21 This study proposed to use the nonsolvent thermally induced phase separation (NTIPS)  
22 method to fabricate a novel Janus membrane for MD applications. The as-prepared  
23 dual-layer membrane consisted of a thin hydrophobic PVDF top-layer and a relatively  
24 thick hydrophilic PVDF-PVA sub-layer. By adopting a facile one-step co-casting  
25 technique and water soluble diluent  $\epsilon$ -caprolactam (CPL), delamination-free dual-layer  
26 membrane was obtained. The SEM morphologies and FTIR crystalline analyses  
27 suggested the membrane formation mechanisms, where the hydrophobic top-layer was  
28 formed via NTIPS process, resulting in an ultra-thin dense skin with finger-like pores  
29 formed beneath; while the hydrophilic sub-layer was induced by TIPS, producing  
30 highly porous cellular structure with high degree pore interconnectivity. Combining the  
31 structural observation and MD performance results, suitable fabrication parameters  
32 were identified as a PVDF concentration of 15 wt% for the hydrophobic layer and  
33 coagulation temperature between 20-40 °C. The total membrane thickness was  
34 optimized as 100-150  $\mu\text{m}$ , given the thickness of hydrophobic layer kept within an  
35 optimal range of 30-60  $\mu\text{m}$  to ensure minimal mass transfer resistance. The Janus  
36 membrane exhibited stable salt rejection above 99.5% over continuous MD runs and  
37 superior permeation flux up to  $165.3 \text{ kg}\cdot\text{m}^{-2}\cdot\text{h}^{-1}$  at 80 °C, which was remarkably higher  
38 than reported MD membranes.

39

40 **Keywords:**

41 Janus membrane; Nonsolvent thermally induced phase separation (NTIPS); Co-coating;  
42 Delamination-free; Direct contact membrane distillation

43

44

## 45 **1. Introduction**

46 Membrane distillation (MD), an emerging membrane technology for seawater  
47 desalination, wastewater treatment and resource recovery applications, is driven by a  
48 vapor pressure difference resulted from the temperature difference across a  
49 hydrophobic membrane [1, 2]. Compared to traditional separation processes such as  
50 thermal distillation or reverse osmosis, membrane distillation is potentially cost  
51 effective due to its ability to incorporate low-grade waste heat and/or renewable energy.  
52 However, MD has achieved limited commercialization mainly due to the challenges  
53 associated with inadequate membranes and process control. These include the trade-  
54 off relationship between low permeability and unavoidably high conductive heat  
55 loss, and liquid intrusion into membrane pores (wetting) which will completely  
56 terminate the operation. To avoid pore wetting, the membrane needs hydrophobic  
57 properties and high liquid entry pressure (LEP) to maintain vapor-filled pores.  
58 Amongst the commonly used polymer materials for making MD membranes, poly  
59 (vinylidene fluoride) (PVDF) is most versatile with its hydrophobic properties and  
60 could be used as either bulk membrane or substrate via various fabrication methods,  
61 such as conventional nonsolvent induced phase separation (NIPS) [3] and thermally  
62 induced phase separation (TIPS) [4], as well as the recently proposed nonsolvent-  
63 thermally induced phase separation (NTIPS, also referred to as combined NIPS and  
64 TIPS) [5, 6]. The requirements to suitable structural characteristics for MD applications  
65 have driven the developments of specialized membranes [7, 8].

66 In direct contact membrane distillation (DCMD), high mass transfer and low  
67 heat transfer are preferred to enhance the vapour permeation flux and maintain the  
68 driving force arising from the temperature difference [9]. Therefore, effective mass  
69 transport coefficients require relatively porous and thin membranes to achieve high  
70 permeability; while high thermal efficiency and physical robustness come from  
71 thick membranes. To address this issue, it is preferable to reduce the vapour transport  
72 distance via a possibly thin hydrophobic layer; while maintain the overall membrane  
73 thickness via a thick hydrophilic layer to reduce conductive heat loss and  
74 temperature polarization effect [8,10,11]. A membrane with hydrophobic/  
75 hydrophilic dual-layer structure can be considered as a Janus membrane, whose key  
76 feature is the opposing properties of both surfaces such as hydrophobicity and  
77 hydrophilicity, or positive and negative charges [12]. Since 1982 the concept of Janus

78 membrane was first introduced to MD by Cheng and Wiersma [13], there is a surge of  
79 interest on developing membranes with asymmetric wettability for MD [9,12], *i.e.*,  
80 hydrophobic/ hydrophilic dual-layers. Hydrophobicity is a surface property  
81 influenced by many factors such as surface chemistry, roughness and porosity. The  
82 characterization of hydrophobicity is commonly through measuring the contact angle  
83 of water ( $CA_w$ ), where  $65^\circ$  has been defined as the boundary between hydrophilicity  
84 ( $CA_w < 65^\circ$ ) and hydrophobicity ( $CA_w > 65^\circ$ ) based on the difference in the structure  
85 of interfacial water [14,15]. Khayet et al. [16] reported a series of Janus composite  
86 membranes using polyetherimide (PEI) substrate modified by fluorinated surface  
87 modifying macromolecules (SMM). These membranes were fabricated by conventional  
88 phase inversion method using solvent N,N- dimethylacetamide and non-solvent  $\gamma$ -  
89 butyrolactone (GBL) and exhibited the characteristics of hydrophobic/hydrophilic  
90 structure. The membranes were tested [8,17] and showed 2 times higher membrane flux  
91 in DCMD at  $45^\circ\text{C}$  compared to commercial PTFE membranes. Based on the  
92 experimental work, Qtaishat et al. [11] proposed the guidelines for preparing high flux  
93 dual-layer MD membranes through mathematical modeling. Figoli et al. [18] developed  
94 a hydrophobically coated membrane through dip-coating method, consisting of a top  
95 thin hydrophobic layer casted on the commercial hydrophilic membrane. Bonyadi et  
96 al.[19] first applied a co-extrusion method to fabricate hydrophobic/hydrophilic  
97 composite hollow fibers, which obtained a flux as high as  $55\text{ kg}\cdot\text{m}^{-2}\cdot\text{h}^{-1}$  at  $90^\circ\text{C}$  in  
98 DCMD. Edwie et al. [20] also developed hydrophobic/hydrophilic dual-layer hollow  
99 fiber using methanol as a non-solvent additive with the dry-jet wet phase inversion  
100 method, obtaining flux up to  $83.4\text{ kg}\cdot\text{m}^{-2}\cdot\text{h}^{-1}$  in DCMD. Su et al. [21] embedded  
101 graphite particles and multiwall carbon nanotubes (MWNT) into the dual-layer hollow  
102 fiber to improve its thermal conductivity for DCMD by the dry-jet wet-spinning  
103 approach, achieving a significant increase in vapor flux from  $41.2$  to  $66.9\text{ kg}\cdot\text{m}^{-2}\cdot\text{h}^{-1}$ .  
104 Yet, a simpler fabrication method should be sought after to produce robust and high  
105 flux Janus membranes for MD applications.

106 Until now, how to effectively avoid delamination is a crucial question in the  
107 fabrication of high performance dual-layer membranes. In particular, the mechanism of  
108 the adhesion/delamination phenomenon between layers is not well-understood [22]- It  
109 was report that two of the main factors causing layer delamination include variation in  
110 phase inversion rates during phase inversion process and uneven shrinkage rates of

111 different layering materials during membrane formation [23]. Hence, various methods  
112 have been adopted to resolve this issue, such as choice of compatible/miscible polymer  
113 types for the two layers [24], co-extrusion (of hollow fibers) or co-coating techniques  
114 [25], choice of additive (non-solvent) or diluent [26]. However, the above-mentioned  
115 work was mainly focused on hydrophilic/hydrophilic dual-layer membranes. Only a  
116 handful of literature reported on the integration of Janus type of membranes, i.e.,  
117 hydrophobic/hydrophilic [27]. For example, due to the hydrophobic nature of the PVDF  
118 material, its use as the bulk membrane material has posed challenges in hydrophilic  
119 modification via conventional coating or blending methods, most of which may lead to  
120 delamination or leaching of hydrophilic moieties over long-term operation [28]. On the  
121 other hand, some of the modification methods may alter the hydrophilicity of the bulk  
122 membranes [22]. Currently, hydrophilic modifications of PVDF membranes were  
123 mainly applied in ultrafiltration (UF) and microfiltration (MF) processes. For instance,  
124 Vanangamudi et al. [28] fabricated Janus UF membrane by adopting an unconventional  
125 two-step process of electrospinning and subsequent casting, which successfully  
126 overcame the integration problem between the PVDF and chitosan/nylon layers. It was  
127 only recently reported in MD literature [29] that robust and delamination-free dual-  
128 layer hollow fibers could be prepared by manipulating the composition of dope solution  
129 to homogenize the shrinkage rate, such as fabrication conditions and the addition of  
130 Al<sub>2</sub>O<sub>3</sub> nanoparticles into the inner layer dope. However, there is still lack of studies and  
131 understanding on the integration mechanism of hydrophobic and hydrophilic layers and  
132 how it will affect MD performance.

133 This study adopts the NTIPS method for the first time to fabricate a novel Janus  
134 composite membrane for enhanced MD performance. The prepared composite  
135 membrane consists of a hydrophobic PVDF top-layer and a hydrophilic PVDF/PVA  
136 sublayer. Delamination-free integration between the two layers is obtained mainly due  
137 to the use of water soluble diluent  $\epsilon$ -caprolactam (CPL) and a facile one-step co-casting  
138 technique during membrane fabrication. The formation mechanisms of the PVDF top-  
139 layer and PVDF/PVA sub-layer were studied via morphological and crystalline analyses.  
140 The membrane pore structure was optimized by manipulating various fabrication  
141 parameters including casting thickness, PVDF concentration and coagulation  
142 temperature. The as-prepared membranes were tested in direct contact MD (DCMD)  
143 mode to investigate the optimal characteristics of Janus MD membranes.

144

## 145 **2. Experimental**

### 146 2.1. Material and chemicals

147 The commercial polymer poly(vinylidene fluoride) (PVDF, Model: 1015) was  
148 supplied by Solvay Co. The polyvinyl alcohol (PVA, Model: 1788) obtained from  
149 Aladdin Industrial was used as the hydrophilic copolymer. The  $\epsilon$ -Caprolactam (CPL)  
150 and sodium chloride (NaCl, 99.5%) purchased from Sinopharm Reagent Inc. China.  
151 The CPL was used as the diluent for the dope solution and NaCl was the model salt for  
152 synthetic seawater.

153

### 154 2.2. Preparation of PVDF/PVDF-PVA Janus membranes

#### 155 2.2.1. Preparation of dope solutions

156 Dope solution for hydrophobic top-layer: A series of PVDF polymer dope  
157 solutions with various concentrations  $C_d$  ranging from 12 wt% to 20 wt% were prepared  
158 by dissolving PVDF into CPL at 150 °C under nitrogen protection for 1h, then the  
159 mixtures were stirred mechanically for 3h to form homogeneous solutions. The dope  
160 solutions were degassed at the same temperatures to avoid bubbles before casting.

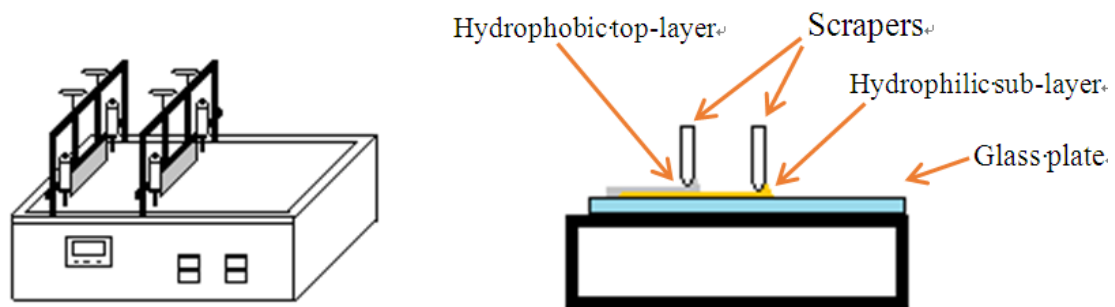
161 Dope solution for hydrophilic sub-layer: based on a previous study on PVDF/PVA  
162 membranes [30], in this study a dope solution containing PVDF, PVA and CPL in a  
163 fixed weight ratio of 12.8: 3.2: 84 was prepared. The PVDF and PVA were dissolved  
164 into CPL at 150 °C under nitrogen protection and mechanical stirring for 2h to become  
165 homogeneous. The solution was then degassed before use.

166

#### 167 2.2.2. Co-casting of composite membrane

168 By maintaining the predetermined temperature (150 °C), the two dope solutions  
169 were casted simultaneously via a co-casting technique [31] by an automated high-  
170 temperature casting machine with two separate casting knives/scrapers which can  
171 control the total thickness  $\delta_d$  of the dual-layer PVDF/PVDF-PVA membrane (Model:  
172 FM-7, Ningbo Gaotong Membrane Apparatus Factory, China), as shown in Figure 1.  
173 There are four steps involved in the co-casting of the proposed Janus composite  
174 membrane: (1) adjust the gap height between the casting knives and glass plate (0 to  
175 400  $\mu\text{m}$ ) by the two scrapers to control the respective thickness of each casting layer;  
176 (2) place the two dope solutions in the respective position of the machine; (3) switch  
177 on the machine to start scraper movement in the same pace to cast both dope solutions

178 simultaneously; (4) immerse the casted dual-layer membrane in the coagulant bath at a  
179 predetermined temperature  $T_c$  (5 -60 °C) to complete the casting step. Finally, the wet  
180 membranes were immersed in deionized (DI) water at room temperature for 24 hours,  
181 allowing complete solvent exchange to remove residual CPL. The obtained membranes  
182 were then frozen in a refrigerator for 12 hours and dried in a freeze drier (SCIENZT-  
183 10N, Ningbo Scientz Biotechnology Co., Ltd) for an additional 12 hours before MD  
184 testing. To ensure reproducibility of experimental data, the same co-casting conditions  
185 were repeated three times to obtain each membrane.



186

187 Figure 1. Schematic diagram for automatic casting machine and co-casting procedure

188

### 189 2.3. Preparation of single-layer PVDF membrane

190 The single-layer PVDF membrane was also prepared by NTIPS to compare against  
191 the structure and performance of the Janus membrane. A series of PVDF polymer dope  
192 solutions with various concentrations  $C_p$  ranging from 12 wt% to 20 wt% were prepared  
193 by dissolving PVDF into CPL at 150 °C into 20 °C coagulation bath. The membrane  
194 thickness  $\delta_p$  of the single-layer PVDF membrane can be controlled through casting. The  
195 details of single-layer PVDF membrane preparation can be found in the previous work  
196 [5].

197

### 198 2.4. Membrane Characterization

199 The top/bottom surface and cross-sections of dual-layer flat sheet membrane were  
200 observed using a scanning electron microscope (SEM, NOVA NANOSEM 450, FEI,  
201 Hillsboro, USA). Prior to the scan, membrane samples were immersed in liquid  
202 nitrogen, fractured and then coated with platinum using a coater (VACUUM DEVICE  
203 MSP-1S). ATR-FTIR (Agilent Cary 660) was used to analyze the functional groups in  
204 the top and bottom skin layers of the membrane. The penetration depth of the ATR-  
205 FTIR is a few microns and hence can obtain the crystalline structural information of the

206 membrane [32].

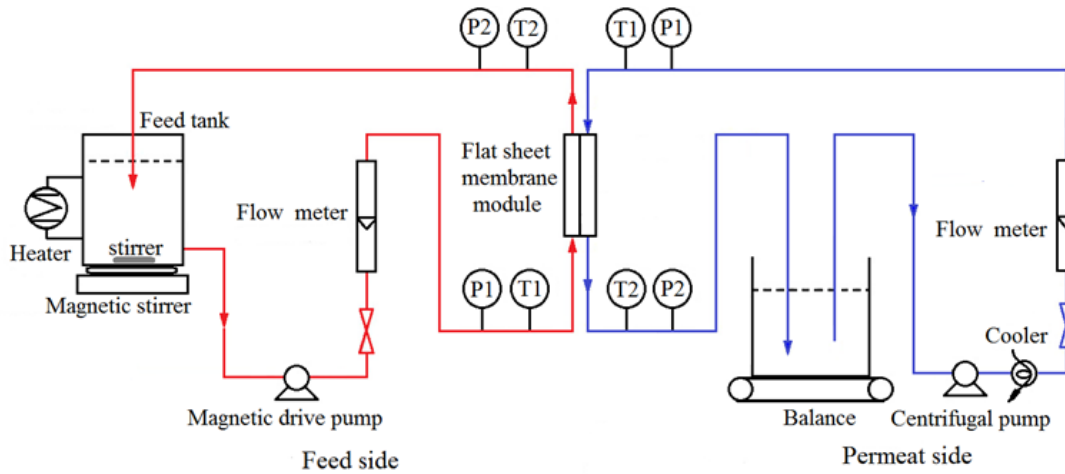
207 The overall membrane porosity ( $\epsilon$ ) was calculated from the ratio of the pore  
208 volume to the total volume of the membrane. The membrane pore volume was  
209 determined by measuring the dry and wet weights of membrane using IPA as a wetting  
210 agent [5, 33]. The measurement of liquid entry pressure of water ( $LEP_w$ ) of the  
211 membranes was conducted using a customized setup with synthetic seawater (i.e., 3.5  
212 wt% NaCl solution, conductivity  $\sim 60 \text{ ms} \cdot \text{cm}^{-1}$ ) as the testing liquid on the feed side and  
213 DI water (conductivity  $< 10 \text{ } \mu\text{s} \cdot \text{cm}^{-1}$ ) as the reference at the permeate side to detect the  
214 occurrence of pore wetting. During testing, the pressure of the NaCl solution side was  
215 increased steadily using compressed  $\text{N}_2$  gas, by 0.01 MPa increments in every 15 min.  
216 The pressure at which a drastic initial increase on the conductivity of the permeate side  
217 and a continuous conductivity increase was taken as the LEP. The conductivity of the  
218 solution was monitored by a conductivity meter (DDSJ-308A, INESA Instrument). The  
219 mean pore size ( $r_m$ ) was determined and calculated based on the DI water filtration  
220 velocity method [34]. The tensile properties ( $\sigma_m$ ) of the membranes were measured via  
221 tensile strength using a tensiometer (Model: 5542, Instron Corp., Boston, MA, USA).  
222 Five membrane samples under same condition were tested to ensure reproducibility.  
223 The contact angles of water ( $CA_w$ ) of both surfaces of the as-prepared membranes were  
224 measured by a Goniometer (model: Kruss DSA100, Hamburg, Germany). Five spots of  
225 each membrane were tested and the average of measured values is reported.

226

## 227 2.5. Direct contact membrane distillation (DCMD) performance testing

228 To evaluate the performance of the as-prepared PVDF/PVDF-PVA Janus  
229 membranes, DCMD experiments were conducted through a laboratory setup, as  
230 illustrated in Figure 2. The effective membrane area was  $10 \times 10^{-4} \text{ m}^2$  and the  
231 hydrophobic top-layer of the membrane was in contact with the hot feed solution  
232 (synthetic seawater: 3.5 wt% NaCl); while the hydrophilic sub-layer faced towards the  
233 permeate side with DI water. The feed solution was heated in the range of  $50 \sim 80 \text{ }^\circ\text{C}$   
234 and recirculated with a flow rate of 110 L/h by a magnetic drive pump; while the  
235 permeate was cooled to  $17.5 \text{ }^\circ\text{C}$  with a flow rate of 110 L/h by a centrifugal pump. The  
236 linear velocities of both feed and permeate sides were identical as 0.61 m/s and the  
237 corresponding Reynolds number ( $Re$ ) is approximately 4000. The feed and permeate  
238 were recirculated through both sides of the modules in counter-current mode. The  
239 continuous weight gain of the collected distillate was measured using a digital balance

240 (EK-2000i, A&D Co. Ltd.). The electrical conductivity of the permeate stream was  
 241 monitored by the conductivity meter to calculate salt rejection. For each membrane,  
 242 DCMD experiments were repeated three times to ensure reproducibility.



243  
 244 Figure 2 Schematic diagram for direct contact membrane distillation (DCMD)  
 245 experimental setup  
 246

247 The MD permeation flux for each feed temperature was calculated using Eq. (1):

$$248 \quad J = \frac{\Delta W}{A \cdot t} \quad (1)$$

249 where  $J$  is the permeation flux in  $\text{kg} \cdot \text{m}^{-2} \cdot \text{h}^{-1}$ ,  $\Delta W$  is the permeation weight  
 250 automatically collected over a pre-determined period of time, in kg,  $t$  in hour, and  $A$  is  
 251 the effective permeation area, in  $\text{m}^2$ .

252 The rejection  $R$  was calculated according to the following equation:

$$253 \quad R = \frac{C_f - C_p}{C_f} \times 100\% \quad (2)$$

254 where  $C_f$  and  $C_p$  are the concentration of the feed and permeate, respectively.

### 255 3. Results and Discussion

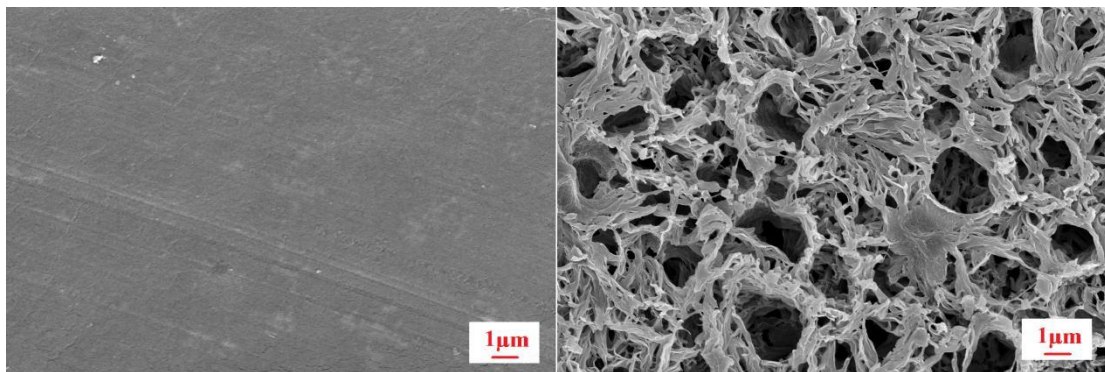
#### 256 3.1 NTIPS membrane morphology and phase separation mechanism

257 Figure 3 illustrates the typical morphologies of the top/bottom surface and cross-  
 258 section of the as-prepared Janus PVDF/PVDF-PVA membrane with 15wt% PVDF  
 259 concentration in the hydrophobic layer. As shown in Figure 3(a)-(b), the surface

260 morphologies of the hydrophobic top-layer and hydrophilic sub-layer of the membrane  
261 are significantly different, i.e., the top surface is smooth and dense with no macropores  
262 (10,000 $\times$ ); while the bottom surface exhibits highly porous structure (10,000 $\times$ ). In  
263 Figure 3(c)-(f) the cross-section SEM images of membrane clearly show that the  
264 asymmetric structure consists of two layers with distinct interface between the  
265 hydrophobic top-layer and hydrophilic sub-layer (Figure 3(c) (800 $\times$ )). In the enlarged  
266 images of Figure 3(d) (2500 $\times$ ) &(e) (10,000 $\times$ ), the hydrophobic top-layer (thickness of  
267  $40\pm 10\ \mu\text{m}$ ) exhibits an ultra-thin dense skin (0.5  $\mu\text{m}$ ) with finger-like macrovoids and  
268 bicontinuous network formed beneath, which is similar to the asymmetric structure of  
269 the NTIPS membranes prepared in our previous work [5]. On the contrary, the PVDF-  
270 PVA hydrophilic sub-layer shows a relatively homogenous and highly porous cellular-  
271 like pore structure with large pore size in the range of 1-3  $\mu\text{m}$ , as shown in Figure 3(f)  
272 (10,000 $\times$ ). The pores are highly connected forming a bicontinuous network. Overall,  
273 although a distinct interface is observed between the hydrophobic and hydrophilic  
274 layers, no delamination occurs due to the high degree of interconnectivity of pores in  
275 the transitional region, as shown in Figure 3(e). This can be mainly explained by the  
276 minimal interfacial resistance between the two layers due to use of same diluent CPL.  
277 Also, the two layers (PVDF and PVDF-PVA (8:2)) show strong adhesiveness due to  
278 the use of same bulk polymer.

279 The morphological results can be explained by the combined NIPS and TIPS  
280 mechanisms governing the formation of such dual-layer structure of the PVDF/PVDF-  
281 PVA membrane. In the hydrophobic layer the asymmetric structure, i.e., ultra-thin dense  
282 skin and finger-like pores, is mainly formed through the NIPS mechanism, and the  
283 bicontinuous network beneath the skin is created via TIPS. This is because that the  
284 dense skin is formed due to the rapid quenching into the coagulation bath; while the  
285 finger-like microvoids underneath is generated attributed to the relatively rapid  
286 exchange of water (non-solvent) and CPL diluent, mainly following the NIPS  
287 mechanism. On the other hand, the bicontinuous network pore of the hydrophobic layer  
288 is a typical structure formed by TIPS. Hence, the characteristic structure and  
289 morphology of the hydrophobic top-layer are consistent with the NTIPS membranes

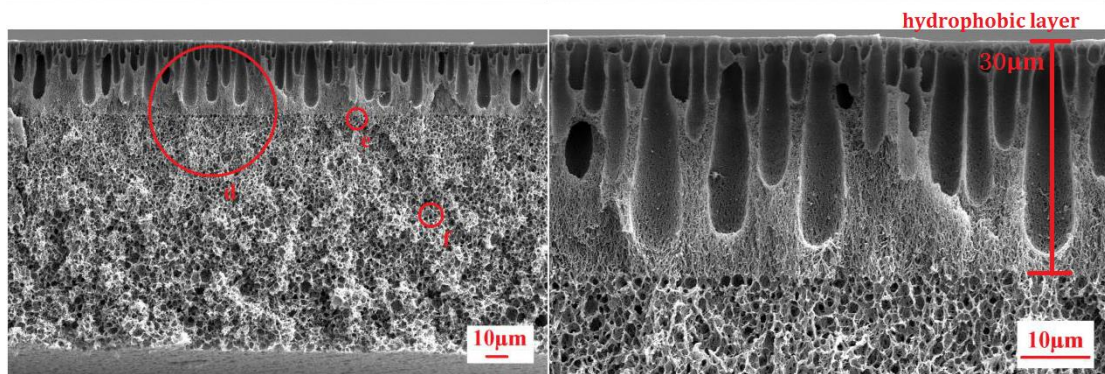
290 developed previously [5]. The homogeneous cellular-like pore structure of the  
 291 hydrophilic layer can be attributed to the TIPS formation mechanism. This is due to the  
 292 generally much faster heat transfer rate (dominant in TIPS) in the dope leading to the  
 293 phase separation and crystallization in the polymer-rich phase, and eventually the  
 294 formation of the cellular-like pores, which is similar to the typical bulk structure of  
 295 hydrophilically modified PVDF/PVA membrane fabricated via TIPS process in the  
 296 previous work [30].



297  
 298

(a) Top surface (10,000×)

(b) Bottom surface (10,000×)

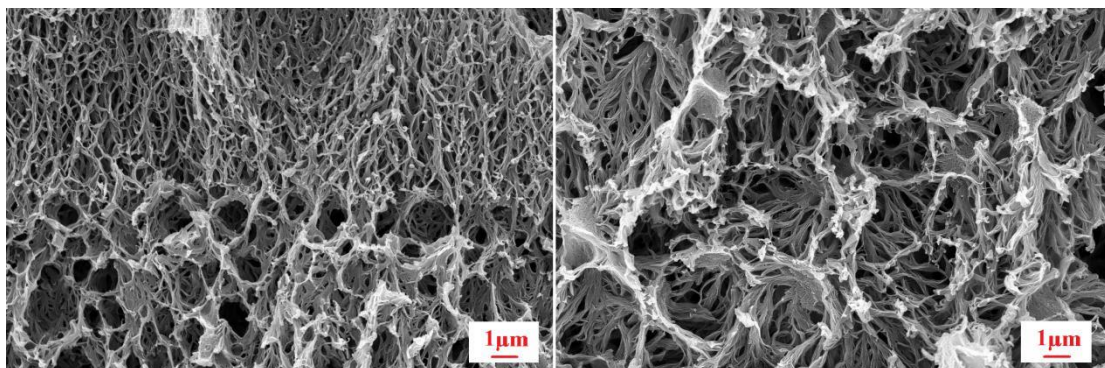


299

300

(c) Whole cross-section (800×)

(d) Cross section of hydrophobic layer (2500×)



301

302

(e) Cross section of interface (10,000×)

(f) Cross section of hydrophilic layer (10,000×)

303 Figure 3 Surface and cross-section morphology of hydrophobic/hydrophilic dual-layer  
 304 PVDF/PVDF-PVA membranes (membrane fabrication parameters:  $C_d=15$  wt%,  $\delta_d$

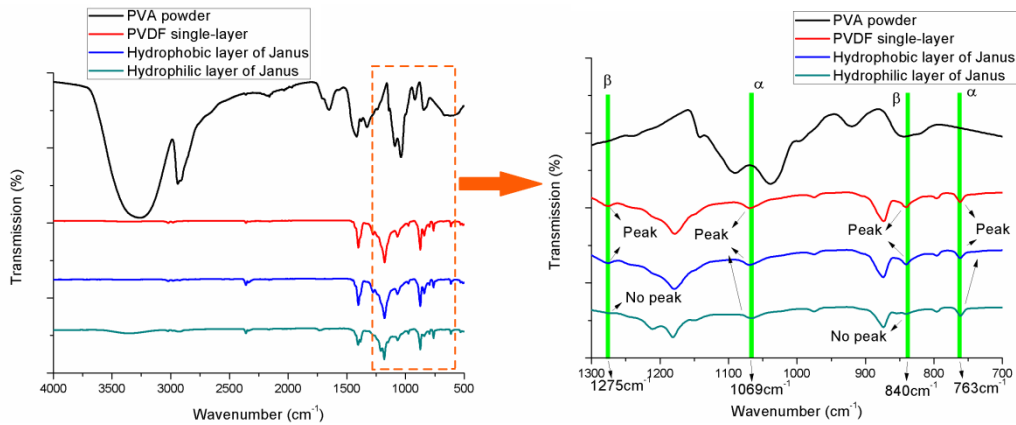
=150  $\mu\text{m}$ ,  $T_c = 20\text{ }^\circ\text{C}$ .)

305

306

307 To further investigate the phase separation mechanism during the formation of the  
308 PVDF/PVDF-PVA Janus membrane, the PVDF crystalline structural information in the  
309 top/bottom skin layers was obtained via ATR-FTIR. The resulting spectrum are shown  
310 in Figure 4, in which the left figures shows the full spectra of the hydrophilic and  
311 hydrophobic layers in comparison to the reference peaks of pure single-layer PVDF  
312 membrane prepared by NTIPS. The scan of the pure PVA powder was to ensure that its  
313 characteristic peaks would not interfere with that of the PVDF crystalline. While the  
314 right figure in Figure 4 gives the enlarged window between wave length of 1300 and  
315  $700\text{ cm}^{-1}$ .

316 Generally, the IR absorption bands at approximately 1211, 1149, 1069, 975, 854,  
317 794, and  $763\text{ cm}^{-1}$  represent the characteristic spectrum of an  $\alpha$  phase PVDF crystal  
318 [35]; whereas the absorption bands at 1275 and  $840\text{ cm}^{-1}$  represent the characteristic  
319 spectrum of  $\beta$  phase PVDF[36, 37]. Based on the previous study [5] and discussion for  
320 Figure 3, in the NTIPS process the  $\alpha$  phase crystallization of PVDF is induced by TIPS  
321 and the  $\beta$  phase is induced by NIPS. It is observed in Figure 4 that similar to the pure  
322 single-layer PVDF membrane, the hydrophobic top-layer of the composite membrane  
323 exhibit IR absorption bands at  $840\text{ cm}^{-1}$  ( $\text{CH}_2$  rocking) and  $1275\text{ cm}^{-1}$  ( $\text{CF}_2$  group  
324 symmetrical stretching vibration), as well as  $763\text{ cm}^{-1}$  ( $\text{CF}_2$  bending and skeletal  
325 bending) and  $1069\text{ cm}^{-1}$  (deformation vibration of C-F) [38-40], indicating the  
326 occurrence of both  $\alpha$  and  $\beta$  phase crystallization induced by the NTIPS mechanism.  
327 While the hydrophilic sub-layer of the composite membrane only shows peaks at  $763\text{ cm}^{-1}$   
328 and  $1069\text{ cm}^{-1}$ , indicating the occurrence of  $\alpha$  phase crystallization induced by  
329 TIPS.



330

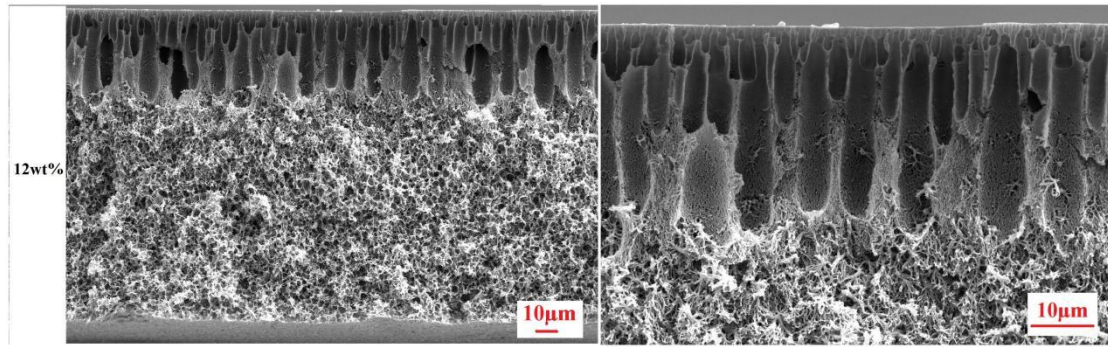
331 Figure 4. FTIR spectra of the different type of membranes, including pure PVA powder,  
 332 pure single-layer PVDF membrane (top-surface), hydrophobic top-layer and  
 333 hydrophilic sub-layer of dual-layer PVDF/PVDF-PVA membrane

334

335 3.2 Effect of fabrication parameters on membrane structure

336 3.2.1 PVDF concentration of hydrophobic top-layer

337 The effect of dope composition on the membrane structure was investigated via  
 338 varying the PVDF concentration of the hydrophobic layer in the range of 12-20 wt%;  
 339 while maintaining constant dope composition of the hydrophilic layer and constant  
 340 overall thickness of 150  $\mu\text{m}$ . Figure 5 displays the cross sectional morphologies of the  
 341 Janus membrane with 12, 15 and 20 wt% PVDF in the hydrophobic layer. Similar to  
 342 the typical morphology shown in Figure 3, all the membranes exhibit an ultra-thin dense  
 343 skin with finger-like macrovoids and bicontinuous network formed underneath.  
 344 However, the finger-like pores in the hydrophobic layer becomes shorter and the  
 345 interface between the hydrophobic and hydrophilic layers is less distinct with the  
 346 increase of PVDF concentration. This is mainly attributed to the increased dope solution  
 347 viscosity, which reduced the CPL/water exchange rate and suppressed the instantaneous  
 348 phase separation beneath the top surface regions. Also, 12 wt% PVDF dope was too  
 349 dilute and may easily lead to defected pore structure; while the 20 wt% PVDF dope  
 350 was too thick to cast smoothly in the co-casting process.

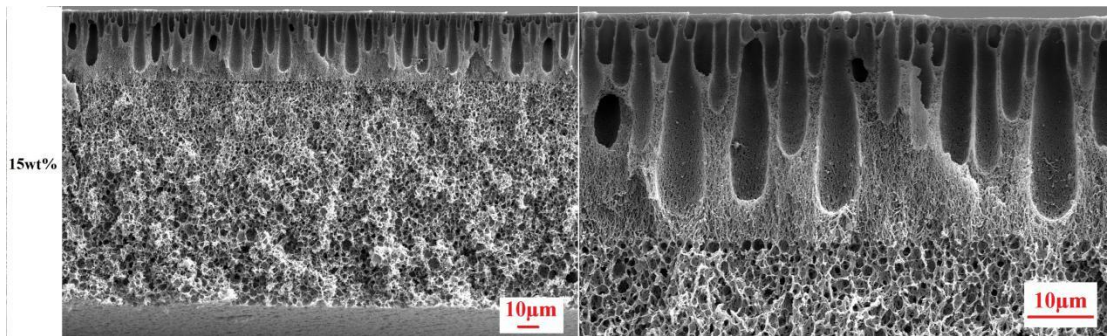


351

352

Whole cross-section (800×)

Cross section of hydrophobic layer (2000×)

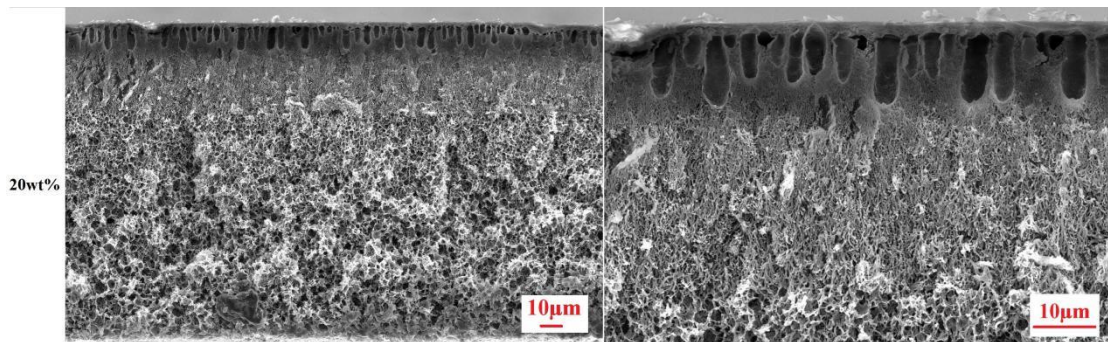


353

354

Whole cross-section (800×)

Cross section of hydrophobic layer (2500×)



355

356

Whole cross-section (800×)

Cross section of hydrophobic layer (2500×)

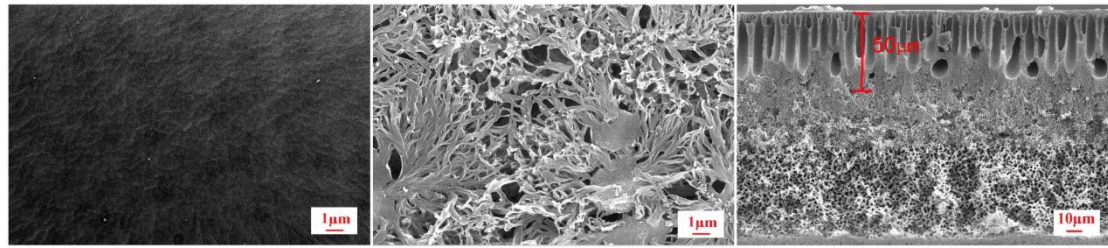
357 Figure 5. Effect of different PVDF concentration of the hydrophobic top-layer on the  
 358 cross section structures of hydrophobic/ hydrophilic dual-layer PVDF/PVDF-PVA flat  
 359 sheet membrane (membrane fabrication parameters:  $\delta_d=150 \mu\text{m}$ ,  $T_c = 20 \text{ }^\circ\text{C}$ )

360

### 361 3.2.2 Coagulation temperature

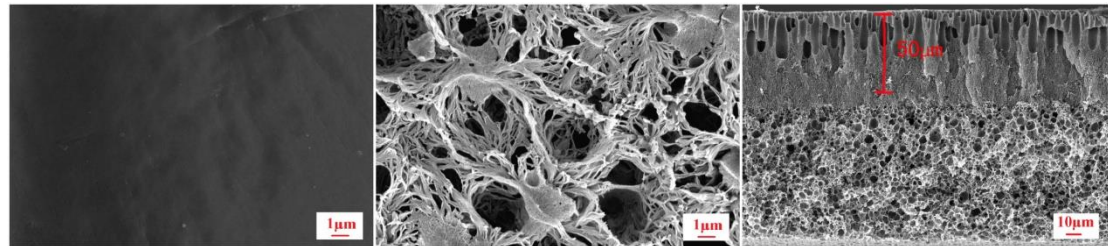
362 The effect of the temperature of water coagulant bath on membrane structure was  
 363 investigated. Figure 6 (a)-(d) shows that SEM image of the top and bottom surfaces,  
 364 and cross section morphologies of the membranes at coagulation temperatures of 5 °C,  
 365 20 °C, 40 °C and 50 °C, respectively. The thickness of the hydrophobic top-layer is  
 366 marked in the SEM images of Figure 6. It is clear that the partial thickness of the top  
 367 layer K is within the range of  $40\pm 10 \mu\text{m}$  at coagulation temperature below 50 °C. The  
 368 respective layer thickness of the Janus membrane was mainly controlled by adjusting





(c) 40 °C

Top surface (10,000×)      Bottom surface (10,000×)      Cross-section (900×)



(d) 50 °C

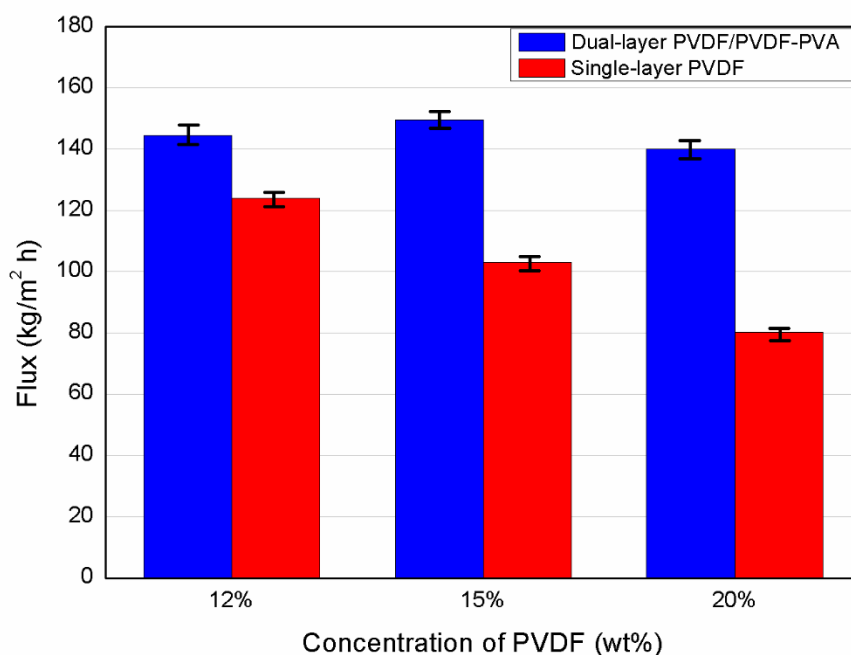
Figure 6. SEM image of the morphology of dual-layer PVDF/PVDF-PVA membranes obtained at various coagulation temperature (membrane fabrication parameters:  $C_d=15$  wt%,  $\delta_d=150$   $\mu\text{m}$ )

### 3.3 Evaluation of DCMD Performance

#### 3.3.1 Effect of fabrication parameters on MD performance

With the PVDF concentration of the hydrophobic layer varied between 12 to 20 wt% and respective total membrane thickness fixed at  $\delta_d=150$   $\mu\text{m}$  (un-optimized) and  $\delta_p=110$   $\mu\text{m}$ , the DCMD performance of the dual-layer Janus and single-layer PVDF membranes was compared in Figure 7. It was found that membrane fluxes of the dual-layer membranes are much higher than that of the single-layer ones, reaching up to  $149.5$   $\text{kg}\cdot\text{m}^{-2}\cdot\text{h}^{-1}$  at feed temperature of  $T_f=80$  °C and permeate temperature of  $T_p=17.5$  °C. This is because that the partial thickness of the hydrophobic layer of the dual-layer membrane is only about  $40\pm 10$   $\mu\text{m}$  (Figure 5), even though the total thickness of the dual-layer membrane is larger than that of the single-layer one, i.e.,  $\delta_d$  of  $150$   $\mu\text{m}$  vs.  $\delta_p$  of  $110$   $\mu\text{m}$ . For the single-layer membrane, the flux decreases drastically from  $124$  to  $80$   $\text{kg}\cdot\text{m}^{-2}\cdot\text{h}^{-1}$  as the PVDF concentration increases from 12 to 20 wt%. This is corresponding to the decreasing porosity of the membrane from 88 % to 82.4 %. On the contrary, for the dual-layer membrane, the flux remains relatively constant regardless of PVDF concentration at such total membrane thickness of  $150$   $\mu\text{m}$ . This is

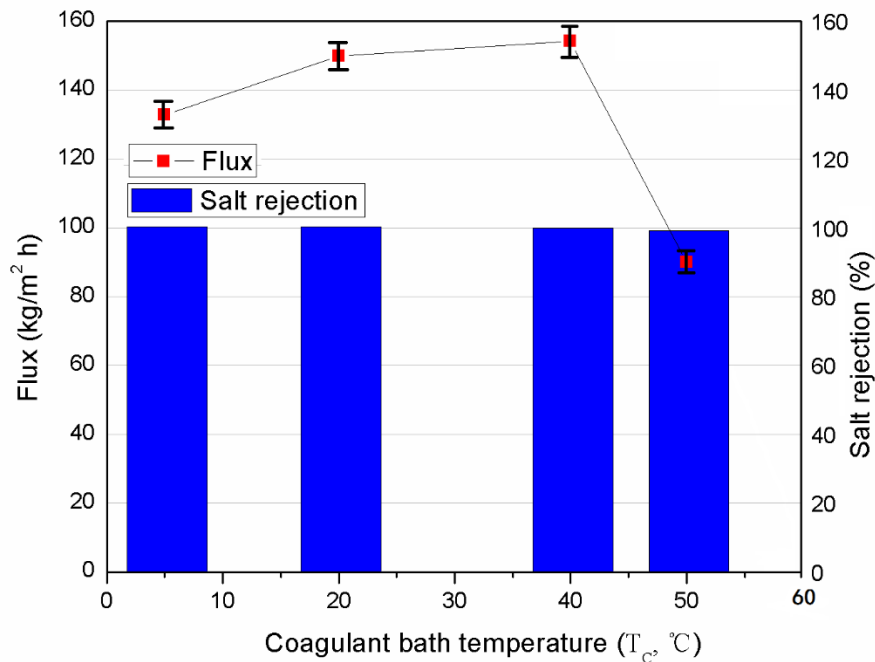
416 also related to the very thin hydrophobic layer, which is consistent with the optimal  
 417 thickness range (30-60  $\mu\text{m}$ ) of the hydrophobic layer reported in MD literature [42].  
 418 Thus the significant advantage of the dual-layer membrane for MD application is easily  
 419 justified. However, taking into account the influence of viscosity of the dope solution  
 420 on membrane fabrication as discussed in Figure 5, an intermediate concentration of 15  
 421 wt% PVDF was chosen as a suitable operating condition. It is noted that the salt  
 422 rejection for all membranes compared in Figure 7 remained above 99.5 %.



423  
 424 Figure 7. Comparison of DCMD performance of Janus and single-layer NTIPS  
 425 membranes at varying PVDF concentration (DCMD parameters:  $T_f=80$  °C,  $T_p=17.5$   
 426 °C; fabrication parameters:  $C_d=12-20$  wt%,  $C_p=12-20$  wt%,  $T_c=20$  °C,  $\delta_d=150$   $\mu\text{m}$ ,  
 427  $\delta_p=110$   $\mu\text{m}$  )

428  
 429 As indicated by the morphological analysis in Figure 6, the variation of  
 430 coagulation temperature  $T_c$  has a significant impact on the membrane structure. Hence,  
 431 the effect of coagulation temperature of the as-prepared Janus membranes was  
 432 investigated in terms of DCMD performance. The results are shown in Figure 8, in  
 433 which an initial increase of membrane flux from 132 to 154  $\text{kg}\cdot\text{m}^{-2}\cdot\text{h}^{-1}$  as  $T_c$  increases  
 434 from 5 to 40 °C and subsequently a dramatic decrease, i.e., from 154 to 89  $\text{kg}\cdot\text{m}^{-2}\cdot\text{h}^{-1}$   
 435 as  $T_c$  increases from 40 to 50 °C, is observed. Meanwhile, the salt rejection maintained  
 436 above 99.7% for the membranes prepared under coagulation temperatures from 5 to 40

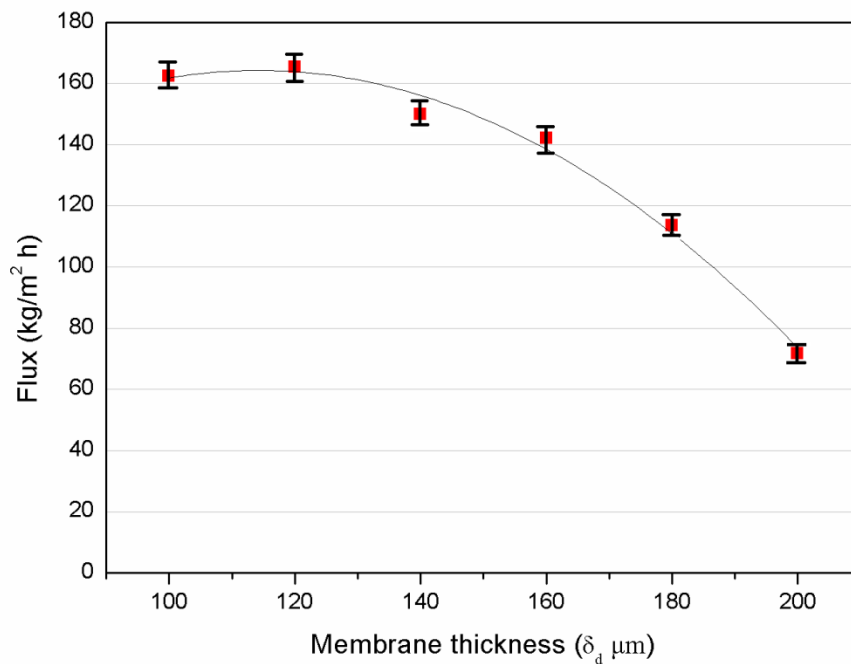
437 °C; while slightly dropped to 99.3% at 50 °C. As explained in Section 3.2.2, the change  
 438 in membrane formation mechanism from TIPS dominant to NIPS dominant as the  
 439 temperature difference between the casted membrane and coagulant bath became  
 440 smaller, causing the membrane to have much longer finger-like pores and denser  
 441 structure in overall. Hence, the membrane permeability has been greatly sacrificed.  
 442 Therefore, a suitable range of coagulation temperature of 20 °C to 40 °C was chosen in  
 443 this work for the fabrication of Janus MD membrane, which is consistent to the  
 444 morphological observations in Figure 6. In addition, considering the minor difference  
 445 in membrane flux between membranes prepared at coagulation temperature of 20 and  
 446 40 °C, 20 °C was chosen as the preferred fabrication condition as it is closer to room  
 447 temperature and thus requires minimal thermal input.



448  
 449 Figure 8. Effect of coagulation temperature on DCMD membrane flux of PVDF/  
 450 PVDF-PVA Janus membrane (DCMD parameters:  $T_f=80$  °C,  $T_p=17.5$  °C; fabrication  
 451 parameters:  $T_c=5$  °C to 50 °C,  $C_d=15$  wt%,  $\delta_d=150$   $\mu$ m)

452  
 453 The optimization of total membrane thickness of the Janus membrane was  
 454 conducted. With the partial thickness of the hydrophobic top-layer kept within  $40\pm 10$   
 455  $\mu$ m, the total membrane thickness  $\delta_d$  was tuned between 100 to 200  $\mu$ m during  
 456 membrane fabrication at a chosen coagulation temperature of 20 °C. The effect of  
 457 membrane thickness on the DCMD performance was investigated and the results are

458 shown in Figure 9. It was found that the permeation flux is up to  $165.3 \text{ kg}\cdot\text{m}^{-2}\cdot\text{h}^{-1}$  at  $\delta_d$   
459 of  $120 \text{ }\mu\text{m}$ . However, it decreases gradually to  $70 \text{ kg}\cdot\text{m}^{-2}\cdot\text{h}^{-1}$  as the  $\delta_d$  continues to  
460 increase to  $200 \text{ }\mu\text{m}$ . The decreasing trend of flux can be explained by the vapor transport  
461 mechanism and temperature profiles through the hydrophobic/hydrophilic dual layer  
462 structure proposed by M. Qtaishat et al [11], the hydrophobic layer is vapor-filled space  
463 while the hydrophilic layer is filled with water in DCMD. The water vapor transports  
464 through the hydrophobic layer of the membrane and condenses at the  
465 hydrophobic/hydrophilic interface. The temperature gradient across the hydrophobic  
466 layer serves as the driving force in MD. With the thickness of the hydrophobic layer  
467 kept constant, the increasing thickness of hydrophilic layer (thus the total membrane  
468 thickness) will lead to an increase of the temperature at the membrane vapor-liquid  
469 interface due to the temperature polarization effect in the hydrophilic layer across the  
470 bulk permeate. Therefore, it will result in a decrease of the MD driving force leading to  
471 decrease in membrane flux. However, the trend of membrane flux vs total thickness  
472 does not follow a linear relationship based on Figure 9. Hence, the ideal membrane  
473 thickness of the Janus membrane can be chosen within the range of  $100$  to  $150 \text{ }\mu\text{m}$  to  
474 simultaneously obtain high flux while maintain a reasonable total membrane thickness  
475 to ensure mechanical robustness, given the partial thickness of the hydrophobic layer is  
476 controlled within the range of  $30$ - $60 \text{ }\mu\text{m}$  to minimize the mass transfer resistance.  
477 Overall the Janus membrane still exhibited high flux of  $110 \text{ kg}\cdot\text{m}^{-2}\cdot\text{h}^{-1}$  even at a large  
478  $\delta_d$  of  $180 \text{ }\mu\text{m}$  (Figure 9), which is higher than compared to its counterpart single-layer  
479 PVDF membrane with a smaller  $\delta_p$  of  $110 \text{ }\mu\text{m}$ , *i.e.*,  $103.2 \text{ kg}\cdot\text{m}^{-2}\cdot\text{h}^{-1}$  (Figure 7). It is  
480 noted that the salt rejection for all membranes discussed in Figure 9 maintained above  
481  $99.5 \%$ .

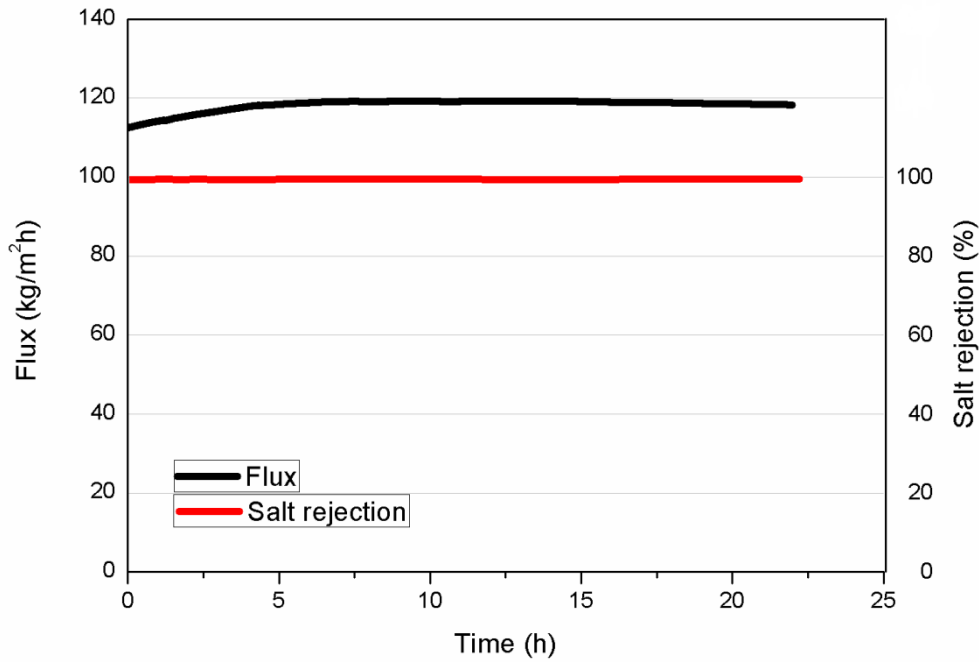


482

483 Figure 9. Optimization of total membrane thickness  $\delta_d$  of dual-layer PVDF/ PVDF-PVA  
 484 membrane in terms of DCMD performance (DCMD parameters:  $T_f=80$  °C,  $T_p=17.5$   
 485 °C; fabrication parameters:  $\delta_d=100\text{-}200$   $\mu\text{m}$ ,  $C_d=15$  wt%,  $T_c = 20$  °C)

486

487 To prove the stability of the membrane in MD, a selected PVDF/PVDF-PVA Janus  
 488 membrane was evaluated in a 22-hour continuous run at a feed temperature of 70 °C.  
 489 The membrane flux and salt rejection are presented in Figure 10. Overall, a stable flux  
 490 of  $118\text{kg}\cdot\text{m}^{-2}\cdot\text{h}^{-1}$  and high salt rejection above 99.5% were obtained during the  
 491 continuous testing, which is a preliminary proof of the membrane stability. It is noted  
 492 that there is a slight fluctuation (within a reasonable error range of 5%) of the membrane  
 493 flux in the initial stage of operation, which is mainly due to the gradual stabilization of  
 494 the operating conditions in DCMD such as the feed and permeate temperatures, as well  
 495 as the hydrodynamics, i.e., flowrates / velocities. When the key parameters of the  
 496 system were established, the flux remained relatively stable during the rest of the MD  
 497 operation as shown in Figure 10.



498  
 499 Figure 10. Continuous DCMD testing of selected Janus PVDF/PVDF-PVA membrane  
 500 (DCMD parameters:  $T_f=70\text{ }^\circ\text{C}$ ,  $T_p=17.5\text{ }^\circ\text{C}$ ; fabrication parameters:  $C_d=15\text{ wt}\%$ ,  
 501  $\delta_d=130\text{ }\mu\text{m}$ ,  $T_c=20\text{ }^\circ\text{C}$  )  
 502

### 503 3.3.2 Characterization of optimal Janus membrane

504 With 15wt% PVDF concentration chosen as the dope composition of the  
 505 hydrophobic layer, coagulation temperature of  $20\text{ }^\circ\text{C}$  and total thickness of  $120\text{ }\mu\text{m}$ , the  
 506 optimal Janus membrane was fabricated by NTIPS method with the one-step co-casting  
 507 technique.

508 Table 1 shows the basic characteristics of the optimal Janus membrane in  
 509 comparison to the single-layer PVDF membrane also prepared by NTIPS, including the  
 510 porosity ( $\epsilon$ ), contact angle of water ( $\theta$ ), LEP of water ( $LEP_w$ ), mean pore size ( $r_m$ ), total  
 511 membrane thickness ( $\delta_d$  for Janus and  $\delta_p$  for single-layer), partial thickness of the  
 512 hydrophobic layer  $K$  and tensile strength ( $\sigma_m$ ). With an overall membrane thickness ( $\delta_d$ )  
 513 of  $120\text{ }\mu\text{m}$ , the as-prepared Janus membrane has a high porosity of 85%. The contact  
 514 angle of water ( $CA_w$ ) of the hydrophilic PVDF-PVA bottom-layer of the Janus  
 515 membrane rapidly decreased to  $0^\circ$ , indicating complete penetration of water into the  
 516 hydrophilic layer of the membrane; while that of the hydrophobic PVDF top-layer was

517 measured stably at  $74\pm 4^\circ$ , which was similar to the  $CA_w$  of the single-layer counterpart  
518 as shown in Table 1. Thus due to the opposing wettability of the top and bottom surfaces,  
519 the membrane can then be classified as Janus-type membrane. The relatively low  $CA_w$   
520 of the hydrophobic layer is due to the smooth surface morphology as shown in Figure  
521 3. Similar  $CA_w$  values of the PVDF membranes designed for MD can be found in the  
522 literature exhibiting stable performance [43]. To measure the anti-wetting properties of  
523 the membrane in MD, LEP<sub>w</sub> is an important parameter and was measured as high as  
524 3.6 bar for the Janus membranes prepared in this study, which is higher than most  
525 reported data in the literature [44,45] indicating its superior ability to resist pore wetting  
526 and sustain stable long-term performance. The single-layer counterpart exhibits similar  
527 porosity and LEP<sub>w</sub> but larger pore size of 34 nm and relatively weaker mechanical  
528 strength. Although the overall thickness ( $\delta_d$ ) of the Janus membrane is slightly larger,  
529 the proportion of the hydrophobic layer is very small, i.e., 30  $\mu\text{m}$ , which is much thinner  
530 than that of the single-layer membrane (110  $\mu\text{m}$ ). Therefore, Janus type membrane has  
531 great potential in MD applications, as it could achieve very thin hydrophobic layer and  
532 thus high permeability; while the addition of thick hydrophilic layer can maintain the  
533 mechanical strength and potentially reduce the conductive heat loss through the  
534 membrane [8,10,11].

535

536 Table 1 Comparison of characterization data of the optimal PVDF/PVDF-PVA dual-  
537 layer and single-layer PVDF membranes ( $C_d = 15 \text{ wt}\%$ ,  $T_c = 20 \text{ }^\circ\text{C}$ )

Membrane type	Porosity ( $\epsilon$ , %)	Contact angle of water, ( $\theta$ , $^\circ$ )		LEP <sub>w</sub> (bar)	Mean pore size ( $r_m$ , nm)	Total thickness ( $\delta_d$ , $\delta_p$ , $\mu\text{m}$ )	K* ( $\mu\text{m}$ )	Tensile strength ( $\sigma_m$ , MPa)
		Top layer	Bottom layer					
		Dual-layer	85 $\pm$ 1					
Single-layer	86 $\pm$ 1	73 $\pm$ 2	/	3.5 $\pm$ 0.1	34 $\pm$ 3	110 $\pm$ 5	110	0.9 $\pm$ 0.1

538 \* K is partial thickness of the hydrophobic layer.

539

### 540 3.3.3 Comparison with other MD membranes

541 A comparison of the as-prepared Janus membrane with other MD flat sheet  
 542 membranes reported in the literature is presented in Table 2 and Figure 11. It was found  
 543 that under similar operating conditions, the dual-layer PVDF/PVDF-PVA membrane  
 544 exhibited superior permeability at optimized thickness of 120  $\mu\text{m}$ , e.g., the flux reached  
 545  $165.3 \text{ kg}\cdot\text{m}^{-2}\cdot\text{h}^{-1}$  with 3.5 wt% NaCl solution and respective feed and permeate  
 546 temperatures of 80 and 17.5  $^{\circ}\text{C}$ . It was plotted in Figure 11 to compare the membrane  
 547 fluxes listed in Table 2 at varying feed temperature from 50 to 80  $^{\circ}\text{C}$ . It is encouraging  
 548 that the as-prepared Janus membrane showed the highest flux, which was at least 60 %  
 549 higher than its single-layer counterpart PVDF membrane also prepared in this work as  
 550 well as other membranes listed. The superior fluxes ( $>120 \text{ kg}\cdot\text{m}^{-2}\cdot\text{h}^{-1}$  at  $T_f=70 \text{ }^{\circ}\text{C}$  and  
 551  $T_p=17.5 \text{ }^{\circ}\text{C}$ , and  $>160 \text{ kg}\cdot\text{m}^{-2}\cdot\text{h}^{-1}$  at  $T_f=80 \text{ }^{\circ}\text{C}$  and  $T_p=17.5 \text{ }^{\circ}\text{C}$ ) obtained with the PVDF-  
 552 PVDF-PVA dual layer membrane is mainly due to the unique asymmetric  
 553 hydrophobic/hydrophilic structure that results in low mass transfer resistance through  
 554 the thin hydrophobic layer. Also, the mechanism of water vapor permeating through the  
 555 hydrophobic layer is considered as Knudsen flow, where the water vapor molecule -  
 556 pore wall collision plays a dominant role in the mass transfer. This is because of the  
 557 small mean pore size of 24 nm, which is below the mean free path of water vapor  
 558 ( $\lambda_w > 139.9 \text{ nm}$ ) [8, 46]. This is consistent with the literature that reported the theoretical  
 559 DCMD flux considering the Knudsen mechanism was generally higher than the flux  
 560 obtained based on the combined Knudsen/molecular diffusion mechanism, where the  
 561 membrane pore size is larger than the mean free path of water vapor [46].

562 Table 2 Comparison of DCMD permeation flux ( $J$ ) between as prepared PVDF/PVDF-  
 563 PVA Janus membrane and other MD membranes reported in literature

Membrane code/material	$J \text{ (kg}\cdot\text{m}^{-2}\cdot\text{h}^{-1})^*$	Operating parameters	Ref.
PVDF HSV 900 modified	83.4	3.5wt.% NaCl; $T_f=80 \text{ }^{\circ}\text{C}$ ; $T_p=17 \text{ }^{\circ}\text{C}$ .	[20]
GO-NBA incorporated membrane	61.9	3.5wt.% NaCl; $T_f=80 \text{ }^{\circ}\text{C}$ ; $T_p=16 \text{ }^{\circ}\text{C}$ .	[47]
PTFE(Carbon	69	3.4wt.% NaCl; $T_f=70 \text{ }^{\circ}\text{C}$ ; $T_p=20 \text{ }^{\circ}\text{C}$	[48]

---

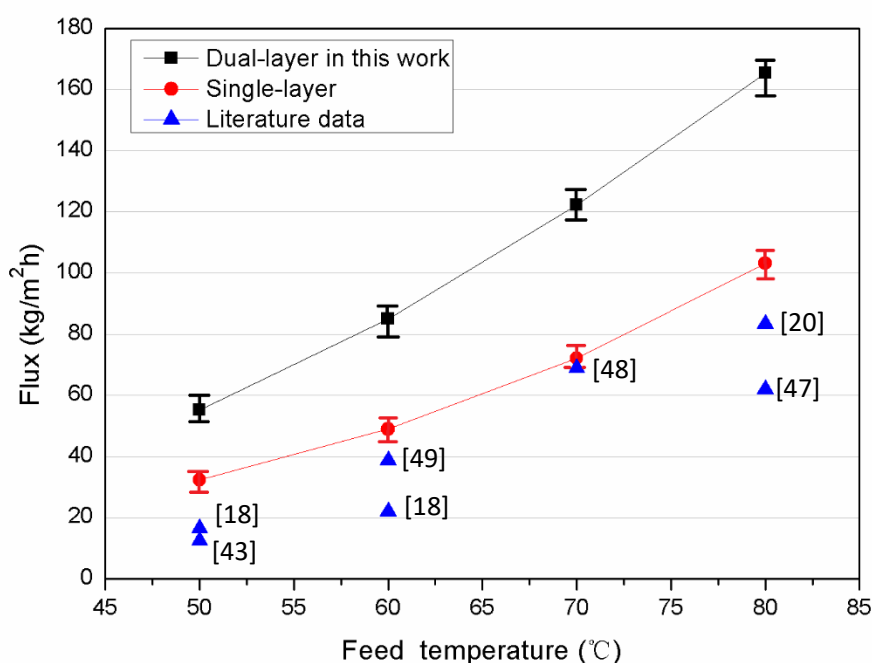
nanotube)				
PFPE- polyamide (commercial)	22	3.5wt.% NaCl; $T_f=60\text{ }^\circ\text{C}$ ; $T_p=14\text{ }^\circ\text{C}$ .	[18]	
PFPE- polyamide (commercial)	16.6	3.5wt.% NaCl; $T_f=50\text{ }^\circ\text{C}$ ; $T_p=14\text{ }^\circ\text{C}$ .	[18]	
PH-TiO <sub>2</sub>	38.7	3.5wt.% NaCl; $T_f=60\text{ }^\circ\text{C}$ ; $T_p=20\text{ }^\circ\text{C}$	[49]	
PVDF/nonwoven fabric composite membrane	12.5	3.5wt.% NaCl; $T_f=50\text{ }^\circ\text{C}$ ; $T_p=20\text{ }^\circ\text{C}$	[43]	
Single-layer PVDF	103.2	3.5wt.% NaCl; $T_f=80\text{ }^\circ\text{C}$ ; $T_p=17.5\text{ }^\circ\text{C}$	This work**	
Dual-layer	55.2	3.5wt.% NaCl; $T_f=50\text{ }^\circ\text{C}$ ; $T_p=17.5\text{ }^\circ\text{C}$ .		
PVDF/PVDF-PVA	85.1	3.5wt.% NaCl; $T_f=60\text{ }^\circ\text{C}$ ; $T_p=17.5\text{ }^\circ\text{C}$ .	This	
	122.2	3.5wt.% NaCl; $T_f=70\text{ }^\circ\text{C}$ ; $T_p=17.5\text{ }^\circ\text{C}$ .	work***	
	165.3	3.5wt.% NaCl; $T_f=80\text{ }^\circ\text{C}$ ; $T_p=17.5\text{ }^\circ\text{C}$ .		

---

564 \* Permeate flux data report in the literature with unit conversion if necessary.

565 \*\* Parameters for single layer membrane:  $C_p=15\text{wt}\%$ ,  $\delta_p=110\mu\text{m}$ ,  $T_c = 20\text{ }^\circ\text{C}$

566 \*\*\* Parameters for dual layer membrane:  $C_d=15\text{wt}\%$ ,  $\delta_d=120\mu\text{m}$ ,  $T_c = 20\text{ }^\circ\text{C}$



567

568 Figure 11. Comparison of DCMD flux as a function of feed temperature of as-prepared  
 569 PVDF-PVDF/PVA Janus, single-layer PVDF and MD membranes reported in literature

570

571

#### 572 4. Conclusions

573 In membrane distillation (MD), the trade-off relationship between the low  
 574 membrane permeability and high conductive heat loss has been recognized as the main  
 575 hurdle for achieving high performance. This study aimed to address this issue by  
 576 fabricating a novel PVDF/PVDF-PVA Janus type membrane via a nonsolvent thermally  
 577 induced phase separation (NTIPS) method.

578 Firstly, delamination-free dual-layer membrane was successfully obtained using a  
 579 one-step co-casting technique and  $\epsilon$ -caprolactam (CPL) as water soluble diluent.  
 580 Combining the SEM morphological analysis and ATR-FTIR crystalline examination,  
 581 the formation mechanism of the membrane was identified: the hydrophobic PVDF top-  
 582 layer was induced mainly by the combined NTIPS process; while the hydrophilic  
 583 PVDF-PVA sub-layer was formed via TIPS. The ultra-thin dense skin of the top-layer  
 584 led to high  $LEP_w$  that ensured high salt rejection and long-term stability of the  
 585 membrane; while the hydrophilic layer exhibited high degree of pore interconnectivity

586 and highly porous structure.

587 Secondly, the membrane structure was influenced by both the PVDF concentration  
588 and coagulation temperature. The increase of PVDF concentration of the hydrophobic  
589 top-layer led to the formation of shorter finger-like pores and lower membrane porosity.  
590 While the increase of coagulation temperature affected both surface and pore structure  
591 of the Janus membrane due to the weakened TIPS but enhanced NIPS mechanism.

592 Thirdly, the Janus membrane demonstrated superior permeability via the DCMD  
593 performance testing. The flux remained relatively constant regardless of the PVDF  
594 concentration of the hydrophobic layer at fixed total membrane thickness, as compared  
595 to its single-layer PVDF counterpart that showed drastic reduction in flux. This was  
596 mainly due to the low mass transfer resistance induced by the thin hydrophobic layer  
597 ( $40\pm 10\ \mu\text{m}$ ) and high porosity. Also, optimal coagulation temperature and overall  
598 membrane thickness were also identified through MD testing. Based on the comparison  
599 with literature data, the Janus membrane showed the highest flux thus far at various  
600 temperature conditions.

601 Overall, the proposed membrane exhibited the desirable robustness and strong  
602 potential in achieving high performance in MD attributing to its unique asymmetric  
603 pore structure and Janus properties.

604

605

## 606 **Acknowledgments**

607 This study was financially supported by the Social Development Research Projects  
608 from Science and Technology Department of Zhejiang Province (No. 2016C33023), the  
609 Natural Science Foundation of Ningbo (No. 2017A610042) and the New-Shoot Talents  
610 Program of Zhejiang Province (No. 2016R405024). This work was also sponsored by  
611 the K.C. Wong Magna Fund from Ningbo University. Xing Yang gracefully  
612 acknowledges the Industry Postdoctoral Fellowship Scheme, Victoria University,  
613 Australia, and Australian Research Council Discovery Project (No. DP170102391).

## 614 **Reference**

615 [1] M.S. El-Bourawi, Z. Ding, R. Ma, M. Khayet, A framework for better understanding membrane  
616 distillation separation process, *Journal of Membrane Science*, 285 (2006) 4-29.

617 [2] M. Khayet, A.O. Imdakm, T. Matsuura, Monte Carlo simulation and experimental heat and mass  
618 transfer in direct contact membrane distillation, *International Journal of Heat & Mass Transfer*, 53 (2010)  
619 1249-1259.

620 [3] S.P. Deshmukh, K. Li, Effect of ethanol composition in water coagulation bath on morphology of  
621 PVDF hollow fibre membranes, *Journal of Membrane Science*, 150 (1998) 75-85.

622 [4] M. Gu, J. Zhang, X. Wang, H. Tao, L. Ge, Formation of poly(vinylidene fluoride) (PVDF) membranes  
623 via thermally induced phase separation, *Desalination*, 192 (2006) 160-167.

624 [5] T. Xiao, P. Wang, X. Yang, X. Cai, J. Lu, Fabrication and characterization of novel asymmetric  
625 polyvinylidene fluoride (PVDF) membranes by the nonsolvent thermally induced phase separation  
626 (NTIPS) method for membrane distillation applications, *Journal of Membrane Science*, 489 (2015) 160-  
627 174.

628 [6] J.T. Jung, J.F. Kim, H.H. Wang, E.D. Nicolo, E. Drioli, Y.M. Lee, Understanding the non-solvent  
629 induced phase separation (NIPS) effect during the fabrication of microporous PVDF membranes via  
630 thermally induced phase separation (TIPS), *Journal of Membrane Science*, 514 (2016) 250-263.

631 [7] E. Drioli, A. Ali, F. Macedonio, Membrane distillation: Recent developments and perspectives,  
632 *Desalination*, 356 (2015) 56-84.

633 [8] M. Khayet, J.I. Mengual, T. Matsuura, Porous hydrophobic/hydrophilic composite membranes:  
634 Application in desalination using direct contact membrane distillation, *Journal of Membrane Science*,  
635 252 (2005) 101-113.

636 [9] H.C. Yang, J. Hou, V. Chen, W. Zhong, Z.K. Xu, Janus hollow fiber membrane with a mussel-inspired  
637 coating on the lumen surface for direct contact membrane distillation, *Journal of Membrane Science*, 523  
638 (2017) 1-7.

639 [10] A. Alkhudhiri, N. Darwish, N. Hilal, Membrane distillation: A comprehensive review, *Desalination*,  
640 287 (2012) 2-18.

641 [11] M. Qtaishat, M. Khayet, T. Matsuura, Guidelines for preparation of higher flux  
642 hydrophobic/hydrophilic composite membranes for membrane distillation, *Journal of Membrane Science*,  
643 329 (2009) 193-200.

644 [12] H.-C. Yang, J. Hou, V. Chen, Z.-K. Xu, Janus membranes: exploring duality for advanced separation,  
645 *Angewandte Chemie International Edition*. 55 (2016) 13398-13407.

646 [13] D.Y. Cheng, S.J. Wiersma, Composite membrane for a membrane distillation system, in, US, Patent,  
647 No. 4,316,772, 1982.

648 [14] Ye Tian and Lei Jiang, Wetting: Intrinsically robust hydrophobicity, *Nature Materials*, 12 (2013)  
649 291-292.

650 [15] Erwin A. Vogler, Structure and reactivity of water at biomaterial surfaces, *Advances in Colloid and*  
651 *Interface Science*, 74 (1998) 69-117.

652 [16] M. Khayet, T. Matsuura, Application of surface modifying macromolecules for the preparation of  
653 membranes for membrane distillation, *Desalination*, 158 (2003) 51-56.

654 [17] M. Khayet, T. Matsuura, M.R. Qtaishat, J.I. Mengual, Porous hydrophobic/hydrophilic composite  
655 membranes preparation and application in DCMD desalination at higher temperatures, *Desalination*, 199  
656 (2006) 180-181.

657 [18] A. Figoli, C. Ursino, F. Galiano, E.D. Nicolò, M.C. Carnevale, A. Criscuoli, Innovative hydrophobic  
658 coating of perfluoropolyether (PFPE) on commercial hydrophilic membranes for DCMD application,  
659 *Journal of Membrane Science*, 522 (2017) 192-201.

660 [19] S. Bonyadi, T.S. Chung, Flux enhancement in membrane distillation by fabrication of dual layer  
661 hydrophilic - hydrophobic hollow fiber membranes, *Journal of Membrane Science*, 306 (2007) 134-146.

662 [20] F. Edwie, M.M. Teoh, T.S. Chung, Effects of additives on dual-layer hydrophobic – hydrophilic  
663 PVDF hollow fiber membranes for membrane distillation and continuous performance, *Chemical*  
664 *Engineering Science*, 68 (2012) 567-578.

665 [21] M. Su, M.M. Teoh, K.Y. Wang, J. Su, T.S. Chung, Effect of inner-layer thermal conductivity on flux  
666 enhancement of dual-layer hollow fiber membranes in direct contact membrane distillation, *Journal of*  
667 *Membrane Science*, 364 (2010) 278-289.

668 [22] G.-d. Kang, Y.-m. Cao, Application and modification of poly(vinylidene fluoride) (PVDF)  
669 membranes &ndash; A review, *Journal of Membrane Science*, 463 (2014) 145 – 165.

670 [23] L. Setiawan, L. Shi, W.B. Krantz, R. Wang, Explorations of delamination and irregular structure in  
671 poly(amide-imide)-polyethersulfone dual layer hollow fiber membranes, *Journal of Membrane Science*,  
672 423-424 (2012) 73-84.

673 [24] Q.C. Xia, J. Wang, X. Wang, B.Z. Chen, J.L. Guo, T.Z. Jia, S.P. Sun, A hydrophilicity gradient  
674 control mechanism for fabricating delamination-free dual-layer membranes, *Journal of Membrane*  
675 *Science*, 539 (2017) 392-402.

676 [25] D. Li, T.-S. Chung, R. Wang, Morphological aspects and structure control of dual-layer asymmetric  
677 hollow fiber membranes formed by a simultaneous co-extrusion approach, *Journal of Membrane Science*,  
678 243 (2004) 155-175.

679 [26] S.P. Sun, K.Y. Wang, N. Peng, T.A. Hatton, T.-S. Chung, Novel polyamide-imide/cellulose acetate  
680 dual-layer hollow fiber membranes for nanofiltration, *Journal of Membrane Science*, 363 (2010) 232-  
681 242.

682 [27] J. Zhu, L. Jiang, T. Matsuura, New insights into fabrication of hydrophobic/hydrophilic composite  
683 hollow fibers for direct contact membrane distillation, *Chemical Engineering Science*, 137 (2015) 79-90.

684 [28] A. Vanangamudi, L.F. Dumée, M.C. Duke, X. Yang, Nanofiber Composite Membrane with Intrinsic  
685 Janus Surface for Reversed-Protein-Fouling Ultrafiltration, *Acs Applied Materials & Interfaces*, 9 (21)  
686 (2017) 18328- 18337.

687 [29] J. Zuo, T.-S. Chung, G.S. O’ Brien, W. Kosar, Hydrophobic/hydrophilic PVDF/Ultem® dual-layer  
688 hollow fiber membranes with enhanced mechanical properties for vacuum membrane distillation, *Journal*  
689 *of Membrane Science*, 523 (2017) 103-110.

690 [30] N. Hu, T. Xiao, X. Cai, L. Ding, Y. Fu, X. Yang, Preparation and Characterization of Hydrophilically  
691 Modified PVDF Membranes by a Novel Nonsolvent Thermally Induced Phase Separation Method,  
692 *Membranes*, 6 (2016) 47.

693 [31] F.J. Fu, S.P. Sun, S. Zhang, T.S. Chung, Pressure retarded osmosis dual-layer hollow fiber  
694 membranes developed by co-casting method and ammonium persulfate (APS) treatment, *Journal of*  
695 *Membrane Science*, 469 (2014) 488-498.

696 [32] M. Bass, V. Freger, Facile evaluation of coating thickness on membranes using ATR-FTIR, *Journal*  
697 *of Membrane Science*, 492 (2015) 348-354.

698 [33] Myoung Jun Park, Ralph Rolly Gonzales, Ahmed Abdel-Wahab, Sherub Phuntsho, Ho Kyong Shon,  
699 Hydrophilic polyvinyl alcohol coating on hydrophobic electrospun nanofiber membrane for high  
700 performance thin film composite forward osmosis membrane, *Desalination*, 426 (2016) 50-59.

701 [34] J. Lv, G. Zhang, H. Zhang, C. Zhao, F. Yang, Improvement of antifouling performances for modified  
702 PVDF ultrafiltration membrane with hydrophilic cellulose nanocrystal, *Applied Surface Science*, (2018),  
703 doi: <https://doi.org/10.1016/j.apsusc.2018.01.256>

704 [35] C. Moazed, Overbey, R. Amp, R.M. Spector, Effect of crystallization temperature on the crystalline  
705 phase content and morphology of poly(vinylidene fluoride). *J Polym Sci Part B Polym Phys*, *Journal of*  
706 *Polymer Science Part B Polymer Physics*, 32 (1994) 859 – 870.

707 [36] Z. Cui, N.T. Hassankiadeh, S.Y. Lee, J.M. Lee, K.T. Woo, A. Sanguineti, V. Arcella, Y.M. Lee, E.  
708 Drioli, Poly(vinylidene fluoride) membrane preparation with an environmental diluent via thermally  
709 induced phase separation, *Journal of Membrane Science*, 444 (2013) 223-236.

710 [37] Y.K. Ong, N. Widjojo, T.S. Chung, Fundamentals of semi-crystalline poly(vinylidene fluoride)  
711 membrane formation and its prospects for biofuel (ethanol and acetone) separation via pervaporation,  
712 *Journal of Membrane Science*, 378 (2011) 149-162.

713 [38] Z. Li, G. Su, D. Gao, X. Wang, X. Li, Effect of Al<sub>2</sub>O<sub>3</sub> nanoparticles on the electrochemical  
714 characteristics of P(VDF-HFP)-based polymer electrolyte, *Electrochimica Acta*, 49 (2004) 4633-4639.

715 [39] A. Salimi, A.A. Yousefi, Analysis Method: FTIR studies of  $\beta$ -phase crystal formation in stretched  
716 PVDF films, *Polymer Testing*, 22 (2003) 699-704.

717 [40] L. Zhu, Y. Wang, F. Hu, H. Song, Structural and friction characteristics of g-C<sub>3</sub>N<sub>4</sub>/PVDF composites,  
718 *Applied Surface Science*, 345 (2015) 349-354.

719 [41] S.A. Mckelvey, W.J. Koros, Phase separation, vitrification, and the manifestation of macrovoids in  
720 polymeric asymmetric membranes, *Journal of Membrane Science*, 112 (1996) 29-39.

721 [42] F. Laganà, G. Barbieri, E. Drioli, Direct contact membrane distillation: modelling and concentration  
722 experiments, *Journal of Membrane Science*, 166 (2000) 1-11.

723 [43] Deyin Hou, Hua Fan, Qinliang Jiang, Jun Wang, Xiaohui Zhang, Preparation and characterization  
724 of PVDF flat-sheet membranes for direct contact membrane distillation, *Separation and Purification  
725 Technology*, 135 (2014) 211-222.

726 [44] M. Khayet, Membranes and theoretical modeling of membrane distillation: a review, *Advances in  
727 Colloid and Interface Science*. 164(2011)56-88.

728 [45] Yuan Liao, Rong Wang, Miao Tian, Chang quan Qiu, Anthony G. Fane, Fabrication of  
729 polyvinylidene fluoride (PVDF) nanofiber membranes by electro-spinning for direct contact membrane  
730 distillation, *Journal of Membrane Science*. 425-426 (2013)30-39.

731 [46] M. Khayet, T.Matsuura, J.I.Mengual, M.Qtaishat, Design of novel direct contact membrane  
732 distillation membranes, *Desalination*, 192 (2006) 105-111.

733 [47] K.J. Lu, J. Zuo, T.S. Chung, Novel PVDF membranes comprising n-butylamine functionalized  
734 graphene oxide for direct contact membrane distillation, *Journal of Membrane Science*, 539 (2017) 34-  
735 42.

736 [48] M. Bhadra, S. Roy, S. Mitra, Flux enhancement in direct contact membrane distillation by  
737 implementing carbon nanotube immobilized PTFE membrane, *Separation & Purification Technology*,  
738 161 (2016) 136-143.

739 [49] S.M. Seyed Shahabadi, H. Rabiee, S.M. Seyedi, A. Mokhtare, J.A. Brant, Superhydrophobic dual  
740 layer functionalized titanium dioxide/polyvinylidene fluoride-co-hexafluoropropylene (TiO<sub>2</sub>/PH)  
741 nanofibrous membrane for high flux membrane distillation, *Journal of Membrane Science*, 537 (2017)  
742 140-150.

743